Drug Delivery with Carbon Nanotubes for *In vivo* Cancer Treatment

Zhuang Liu,[1] Kai Chen,[2] Corrine Davis,[3] Sarah Sherlock,[1] Qizhen Cao,[2] Xiaoyuan Chen,[2] and Hongjie Dai[1]

[1]Department of Chemistry, Stanford University; [2]The Molecular Imaging Program at Stanford, Department of Radiology, Biophysics and Bio-X Program and [3]Department of Comparative Medicine, Stanford University School of Medicine, Stanford, California

Abstract

Chemically functionalized single-walled carbon nanotubes (SWNT) have shown promise in tumor-targeted accumulation in mice and exhibit biocompatibility, excretion, and little toxicity. Here, we show *in vivo* SWNT drug delivery for tumor suppression in mice. We conjugate paclitaxel (PTX), a widely used cancer chemotherapy drug, to branched polyethylene glycol chains on SWNTs via a cleavable ester bond to obtain a water-soluble SWNT-PTX conjugate. SWNT-PTX affords higher efficacy in suppressing tumor growth than clinical Taxol in a murine 4T1 breast cancer model, owing to prolonged blood circulation and 10-fold higher tumor PTX uptake by SWNT delivery likely through enhanced permeability and retention. Drug molecules carried into the reticuloendothelial system are released from SWNTs and excreted via biliary pathway without causing obvious toxic effects to normal organs. Thus, nanotube drug delivery is promising for high treatment efficacy and minimum side effects for future cancer therapy with low drug doses. [Cancer Res 2008;68(16):6652–60]

Introduction

A holy grail in cancer therapy is to deliver high doses of drug molecules to tumor sites for maximum treatment efficacy while minimizing side effects to normal organs (1, 2). Through the enhanced permeability and retention (EPR) effect, nanostructured materials on systemic injection can accumulate in tumor tissues by escaping through the abnormally leaky tumor blood vessels (3–6), making them useful for drug delivery applications. As a unique quasi one-dimensional material, single-walled carbon nanotubes (SWNT) have been explored as novel drug delivery vehicles *in vitro* (7–9). SWNTs can effectively shuttle various biomolecules into cells, including drugs (7–9), peptide (10), proteins (11), plasmid DNA (12), and small interfering RNA (13, 14), via endocytosis (15). The intrinsic near-IR (NIR) light absorption property of carbon nanotubes has been used to destruct cancer cells *in vitro* (16), whereas their NIR photoluminescence property has been used for *in vitro* cell imaging and probing (17). The ultrahigh surface area of these one-dimensional polyaromatic macromolecules allows for efficient loading of chemotherapy drugs (8). Various groups have investigated the *in vivo* behavior of carbon nanotubes in animals (18–20). It is found that well PEGylated SWNTs i.v. injected into mice seem nontoxic over several months (21). Nanotubes accumulated in the reticuloendothelial systems (RES) of mice are excreted gradually via the biliary pathway and end up in the feces (22). Targeted tumor accumulation of SWNTs functionalized with targeting ligands RGD peptide or antibodies has shown high efficiency (18, 20). These results set a foundation for further exploration of carbon nanotubes for therapeutic applications.

In the current work, we show SWNT delivery of paclitaxel (PTX) into xenograft tumors in mice with higher tumor suppression efficacy than the clinical drug formulation Taxol. The water-insoluble PTX conjugated to PEGylated SWNTs exhibits high water solubility and maintains similar toxicity to cancer cells as Taxol *in vitro*. SWNT-PTX affords much longer blood circulation time of PTX than that of Taxol and PEGylated PTX, leading to high tumor uptake of the drug through EPR effect. The strong therapeutic efficacy of SWNT-PTX is shown by its ability to slow down tumor growth even at a low drug dose (5 mg/kg PTX). We observe higher tumor uptake of PTX and higher ratios of tumor to normal organ PTX uptake for SWNT-PTX than Taxol and PEGylated PTX, highly desired for higher treatment efficacy and lower side effect. PTX carried into RES organs by SWNT-PTX is released from the nanotube carriers likely via *in vivo* ester cleavage and is cleared out from the body via the biliary pathway. The non-Cremophor composition in our SWNT-PTX, rapid clearance of drugs from RES organs, higher ratios of tumor-to-normal organ drug uptakes, and the fact that tumor suppression efficacy can be reached at low injected drug dose make carbon nanotube drug delivery a very promising nanoplatform for future cancer therapeutics.

Materials and Methods

Functionalization of SWNTs with phospholipid-branched polyethylene glycol. Raw HiPco SWNTs (0.2 mg/mL) were sonicated in a 0.2 mmol/L solution of DSPE-PEG5000-4-arm-(PEG-amine) (see Supplementary Data for the synthetic chemistry) for 30 min with a cup-horn sonicator followed by centrifugation at 24,000 × *g* for 6 h, yielding a suspension of SWNTs with noncovalent phospholipid-branched polyethylene glycol (PEG) coating in the supernatant (13, 14, 18). Excess surfactant and unreacted PEG molecules were removed by repeated filtration through a 100-kDa molecular weight cutoff (MWCO) filter (Millipore) and extensive washing with water.

PTX conjugation. PTX (LC Laboratories) was modified by succinic anhydride (Aldrich) according to the literature, adding a carboxyl acid group on the molecule at the C-2′-OH position highlighted in Fig. 1*A* (23). SWNTs (300 nmol/L, 0.05 mg/mL) with branched PEG-NH_2 functionalization were reacted with 0.3 mmol/L of the modified PTX (dissolved in DMSO) in the presence of 5 mmol/L 1-ethyl-3-(3-dimethylaminopropyl) carbodiimide hydrochloride (EDC; Aldrich) and 5 mmol/L *N*-hydroxysulfosuccinimide (Sulfo-NHS, Pierce). The solution was supplemented with 1× PBS at pH 7.4. After 6-h reaction, the resulting SWNT-PTX was purified to remove unconjugated PTX by filtration through 5-kDa MWCO filters and extensive washing.

UV-Vis-NIR absorbance spectra of the SWNT-PTX conjugates were measured by a Cary-6000i spectrophotometer. The concentration of SWNTs was determined by the absorbance at 808 nm with a molar extinction coefficient of 7.9 × 10^6 mol/L·cm^{-1} with an average tube length of ~150 nm (16).

Note: Supplementary data for this article are available at Cancer Research Online (http://cancerres.aacrjournals.org/).

Requests for reprints: Hongjie Dai, Department of Chemistry, Stanford University, Stanford, CA 94305. Phone: 650-723-4518; Fax: 650-725-0259; E-mail: hdai@stanford.edu.

doi:10.1158/0008-5472.CAN-08-1468

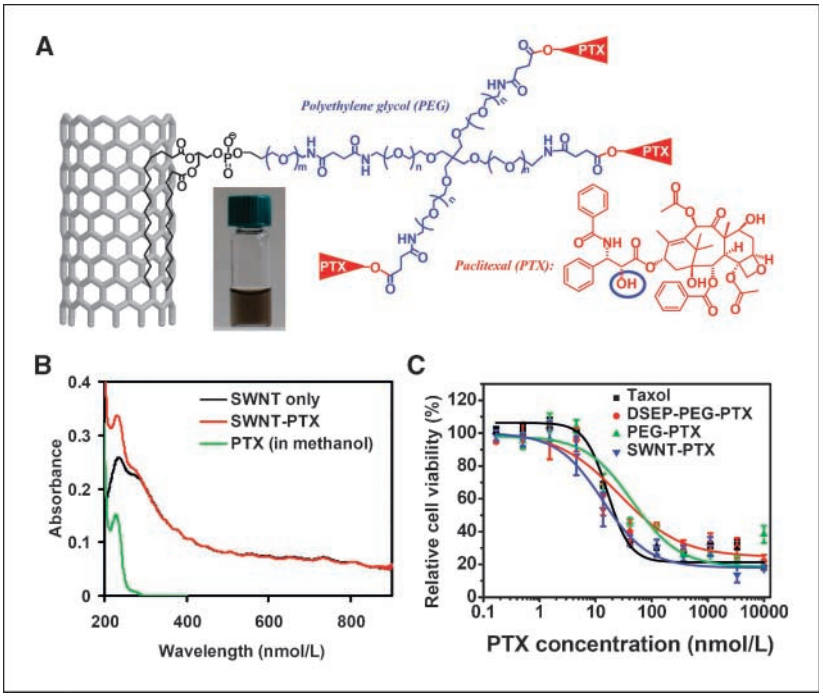

Figure 1. Carbon nanotube for PTX delivery. *A,* schematic illustration of PTX conjugation to SWNT functionalized by phospholipids with branched PEG chains. The PTX molecules are reacted with succinic anhydride (at the circled OH site) to form cleavable ester bonds and linked to the termini of branched PEG via amide bonds. This allows for releasing of PTX from nanotubes by ester cleavage *in vivo*. The SWNT-PTX conjugate is stably suspended in normal physiologic buffer (PBS, as shown in the photo) and serum without aggregation. *B,* UV-VIS-NIR spectra of SWNT before (*black curve*) and after PTX conjugation (*red curve*). The absorbance peak of PTX at 230 nm (*green curve*) was used to measure the PTX loading on nanotubes and the result was confirmed by radiolabel-based assay. Excess unconjugated PTX was removed by extensive filtration and washing. *C,* cell survival versus concentration of PTX for 4T1 cells treated with Taxol, PEG-PTX, DSEP-PEG-PTX, or SWNT-PTX for 3 d. The PTX concentrations to cause 50% cell viability inhibition (IC_{50} values) were determined by sigmoidal fitting to be 16.4 ± 1.7 nmol/L for Taxol, 23.5 ± 1.1 nmol/L for DSPE-PEG-PTX, 28.4 ± 3.4 nmol/L for PEG-PTX, and 13.4 ± 1.8 nmol/L for SWNT-PTX. Error bars based on four parallel samples. Plain SWNTs (no PTX conjugated) are nontoxic (see Supplementary Fig. S4).

Concentration of PTX loaded onto SWNTs was measured by the absorbance peak at 230 nm (characteristic of PTX, Fig. 1*A, green curve*, after subtracting the absorbance of SWNTs at that wavelength) with a molar extinction coefficient of 31.7×10^3 mol/L·cm^{-1}. Note that thorough removal of free unbound PTX was carried out by filtration before the measurement to accurately assess the amount of PTX loaded onto SWNTs. To confirm the PTX loading measured by UV-VIS, ^{3}H-PTX (see the following paragraph) was conjugated to SWNTs. The PTX loading number on nanotubes measured by radioactivity was consistent to that measured by UV-VIS spectra for same batches of samples. The PTX concentration in each batch of SWNT-PTX sample was measured before administration to the mice to ensure the accuracy of dose used in the treatment.

PEGylated PTX (PEG-PTX) and DSPE-PEG-PTX were synthesized by reacting 1 equivalent of 4-arm-(PEG-amine) (10 kDa) or DSPE-PEG5000-4-arm-(PEG-amine) (16 kDa), respectively, with 4 equivalents succinic anhydride–modified PTX in the presence of EDC/NHS at the same reaction condition as conjugation of SWNT-PTX. Excess unreacted PTX was removed by filtration via 5-kDa MWCO filters. The concentrations of PEG-PTX and DSPE-PEG-PTX were measured by its absorbance spectrum. In the case of radiolabeled ^{3}H-PTX, 100 μCi (~5 μg) of ^{3}H-PTX (Moravek Biochemicals) were mixed with 10 mg of regular nonradioactive PTX and used for conjugation to obtain SWNT-PTX or PEG-PTX to impart radioactivity.

Taxol was constituted following the clinical formulation. PTX (6 mg/mL) with or without addition of ^{3}H-PTX (50 μCi/mL, ~2.5 μg/mL) was dissolved in 1:1 (v/v) mixture of Cremophor EL (Aldrich) and anhydrous ethanol (Fisher) and stored at −20°C.

Cell toxicity assay. 4T1 murine breast cancer cell line (from the American Type Culture Collection) was cultured in the standard medium. Cells were plated in 96-wall plates and treated with different concentrations of SWNT-PTX, PEG-PTX, or Taxol for 3 d. Cell viability after various treatments was measured by the 3-(4,5-dimethylthiazol-2-yl)-5-(3-carboxymethoxyphenyl)-2-(4-sulfophenyl)-2H-tetrazolium salt assay with CellTiter 96 kit (Promega).

Animal model and treatment. All animal experiments were performed under a protocol approved by Stanford's Administrative Panel on Laboratory Animal Care. The 4T1 tumor models were generated by s.c. injection of 2×10^6 cells in 50 μL PBS into the right shoulder of female BALB/c mice. The mice were used for treatment when the tumor volume reached 50 to 100 mm^3 (~6 d after tumor inoculation). For the treatment, 150 to 200 μL of different formulations of PTX and SWNTs in saline were i.v. injected into mice via the tail vein every 6 d. The injected doses were normalized to be 5 mg/kg PTX. The tumor sizes were measured by a caliper every other day and calculated as the volume = (tumor length) × (tumor width)^2/2. Relative tumor volumes (Fig. 2) were calculated as V/V_0 (V_0 was the tumor volume when the treatment was initiated).

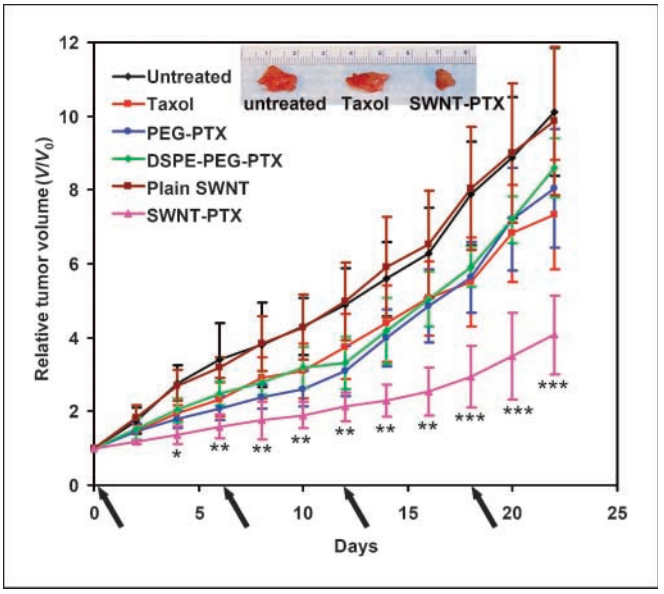

Figure 2. Nanotube PTX delivery suppresses tumor growth of 4T1 breast cancer mice model. Tumor growth curves of 4T1 tumor-bearing mice that received different treatments indicated. The same PTX dose (5 mg/kg) was injected (on days 0, 6, 12, and 18, marked by *arrows*) for Taxol, PEG-PTX, DSEP-PEG-PTX, and SWNT-PTX. *, $P < 0.05$; **, $P < 0.01$; ***, $P < 0.001$, Taxol versus SWNT-PTX. Number of mice used in experiments: 8 mice per group for untreated, 5 mice per group for SWNT only, 9 mice per group for Taxol, 5 mice per group for PEG-PTX, 6 mice per group for DSEP-PEG-PTX, and 14 mice per group for SWNT-PTX. *Inset,* a photo of representative tumors taken out of an untreated mouse (*left*), a Taxol-treated mouse (*middle*), and a SWNT-PTX–treated mouse (*right*) after sacrificing the mice at the end of the treatments.

Tumor slice staining and imaging. Tumor slices (5 μm) were cut after frozen in OCT medium and stained with standard fluorescent terminal deoxynucleotidyl transferase–mediated dUTP nick end labeling (TUNEL), Ki67, and CD31 staining procedures (see details in Supplementary Data). To obtain the Raman mapping image of tumor slices for mice injected with SWNT-PTX, 5-μm-thick paraffin-embedded tumor slices were mounted on SiO_2 substrate and mapped under a Renishaw micro-Raman microscope with a line-scan model (100 mW laser power, 40 μm × 2 μm laser spot size, 20 pixels each line, 2-s collection time, 20× objective). The SWNT G-band Raman intensity was plotted versus X and Y positions across the liver slice to obtain a Raman image.

Pharmacokinetics and biodistribution studies. Blood circulation was measured by drawing ~10 μL blood from the tail vein of tumor-free healthy BALB/c mice after injection of ^{3}H-labeled SWNT-PTX, Taxol, or PEG-PTX. The blood samples were dissolved in a lysis buffer (1% SDS, 1% Triton X-100, 40 mmol/L Tris-acetate, 10 mmol/L EDTA, 10 mmol/L DTT) with brief sonication. Concentration of SWNTs in the blood was measured by a Raman method (22). For ^{3}H-PTX measurement, the blood lysate was decolorized by 0.2 mL of 30% hydrogen peroxide (Aldrich) and the radioactivity was counted by Tri-Carb 2800 TR (Perkin-Elmer) scintillation counter following the vendor's instruction. Blood circulation data were plotted as the blood PTX or SWNT levels with the unit of percentage of injected dose per gram tissue (% ID/g) against time after injection. Pharmacokinetic analysis was performed by first-order exponential decay fitting of the blood PTX concentration data with the following equation: blood concentration = $A \times \exp(-t/\lambda)$, in which A was a constant (initial concentration) and t was the time after injection. The pharmacokinetic variables, including volume of distribution, areas under the curves, and circulation half-lives, are calculated and presented in Supplementary Table S1.

For the biodistribution study, 4T1 tumor-bearing mice (tumor size, ~200 mm^3) were sacrificed at 2 and 24 h after injection of ^{3}H-labeled SWNT-PTX, Taxol, or PEG-PTX. The organs/tissues were collected and split into two halves for ^{3}H-PTX and SWNT biodistribution studies. For the ^{3}H-PTX biodistribution, 50 to 100 mg of tissue were weighed and solubilized in 1 mL of scintillation counting compatible Soluene-350 solvent (Perkin-Elmer) by incubation at 60°C overnight and decolorized by 0.2 mL of 30% hydrogen peroxide. The ^{3}H radioactivity in each organ/tissue was measured by scintillation counting to obtain the biodistribution information of PTX (unit: % ID/g). Note that all the biodistribution and circulation tests were carried out at the treatment dose (normalized to 5 mg/kg PTX).

For SWNT biodistribution, the organs/tissues were wet weighed and homogenized in the lysis buffer (same as used in the blood circulation experiment) with a PowerGen homogenizer (Fisher Scientific). After heating at 70°C for ~2 h, clear homogenous tissue solutions were obtained for Raman measurement as reported previously and described in Supplementary Data (18, 22).

Necropsy, blood chemistry, and histology study. Twenty-four days after initiation of treatment, three mice from each treatment group (SWNT-PTX and Taxol) and two age-matched female BALB/c control mice were sacrificed with blood collected for serum chemistry analysis and organs for histology studies (see details in Supplementary Data).

Statistical analysis. Quantitative data were expressed as mean ± SD. Means were compared using Student's t test. P values of <0.05 were considered statistically significant.

Results

As-grown HiPco SWNTs functionalized by PEGylated phospholipid (14, 18) were used, made by sonication of SWNTs in a water solution of phospholipid-PEG and centrifugation to remove large bundles and impurities. The length distribution of the SWNTs was 20 to 300 nm with a mean of ~100 nm (Supplementary Fig. S1; refs. 14, 18) The PEG functionalized SWNTs exhibited excellent stability without agglomeration in various biological media, including serum (14, 18). We used branched PEG chains for functionalization of SWNTs (see Materials and Methods) to afford more functional amine groups at the PEG termini for efficient drug conjugation (22). PTX was conjugated at the 2′-OH position (23) to the terminal amine group of the branched PEG on SWNTs via a cleavable ester bond (see Materials and Methods), forming a SWNT-PTX conjugate highly soluble and stable in aqueous solutions (Fig. 1*A*). The unconjugated PTX was removed thoroughly from the SWNT-PTX solution by filtration. The loading of PTX on SWNTs was characterized to be ~150 per SWNT with ~100 nm length by radiolabeling method using tritium ^{3}H-labeled PTX and a UV-VIS-NIR optical absorbance (Fig. 1*B*; see Materials and Methods). Dynamic light scattering showed hydrodynamic size of SWNTs before and after PTX conjugation of 120.6 and 132.2 nm, respectively, suggesting no significant aggregation of nanotubes after conjugation of hydrophobic drug molecules. The SWNT-PTX conjugate was found stable in physiologic buffers with little drug release within 48 h (Supplementary Fig. S2). In mouse serum, the release of PTX is faster but SWNT-PTX is still stable for hours (Supplementary Fig. S2), which is much longer than the blood circulation time of SWNT-PTX as described later. *In vitro* cell toxicity tests performed with a 4T1 murine breast cancer cell line found that SWNT-PTX exhibited similar toxicity as Taxol and PEGylated PTX (Fig. 1*C*) without any loss of cancer cell destruction ability. Confocal fluorescence images indicated the endocytosis mechanism of the SWNT-PTX uptake by cells (Supplementary Fig. S3). Consistent to the previous studies (7–14), no noticeable toxic effect to cells was observed for plain nanotube carriers without drug even at high SWNT concentrations (Supplementary Fig. S4).

We next moved to the *in vivo* cancer treatment on the PTX-resistant 4T1 murine breast cancer mice model (24, 25). Female BALB/c mice bearing s.c. inoculated 4T1 tumors were treated with different forms of PTX over several weeks, including the clinical Taxol formulation, PEG-PTX (see Materials and Methods), DSPE-PEG-PTX, and SWNT-PTX (14 mice in this group). The treatments were done by injecting Taxol, PEG-PTX, DSEP-PEG-PTX, and SWNT-PTX (at the same PTX dose of 5 mg/kg for all three formulations, once every 6 days) i.v. into tumor-bearing mice. The mice were observed daily for clinical symptoms and the tumor volume was measured by a caliper every other day. As shown in Fig. 2, a time-related increase in tumor volume was observed in the control untreated group and SWNT vehicle only group in which the tumors showed average fractional tumor volumes (V/V_0) of 10.1 ± 1.7 and 9.8 ± 2.0, respectively, on day 22. Taxol, PEG-PTX, and DSPE-PEG-PTX treatment resulted in V/V_0 of 7.3 ± 1.5 (P = 0.06 versus untreated), 8.0 ± 1.6 (P = 0.18 versus untreated), and 8.6 ± 0.9 (P = 0.33 versus untreated) on day 22, which represents tumor growth inhibition (TGI) of 27.7%, 20.8%, and 14.9%, respectively. In contrast, SWNT-PTX treatment resulted in a V/V_0 of 4.1 ± 1.1 on day 22 ($P = 2.4 \times 10^{-6}$ versus untreated, P = 0.00063 versus Taxol, P = 0.00026 versus PEG-PTX, and $P = 2.7 \times 10^{-5}$ versus DSEP-PEG-PTX), representing a TGI of 59.4%, which is significantly more effective than Taxol, PEG-PTX, and DSPE-PEG-PTX.

To investigate the tumor suppression mechanism, we performed TUNEL assay to examine the apoptosis level in the tumors (26) from mice that received different treatments. Similar to untreated tumor, Taxol-treated tumor showed only 2% to 3% of apoptotic cells (Fig. 3*A*, *1st* and *2nd rows*; Supplementary Fig. S5*A*). In contrast, high apoptosis level (~70%; P < 0.0001 versus untreated and Taxol-treated tumors) was observed in SWNT-PTX–treated tumor (Fig. 3*A*, *4th row*; see Supplementary Fig. S5*A* for quantitative comparison), consistent with the improved TGI efficacy

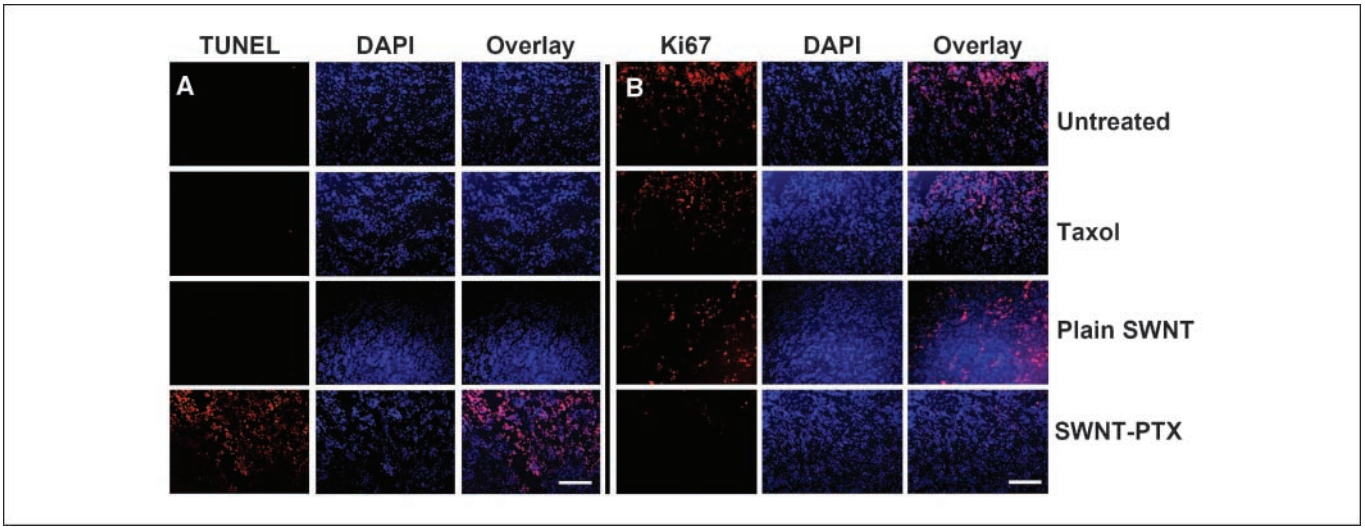

Figure 3. Tumor staining for understanding of treatment effects. *A,* TUNEL (apoptosis assay) and 4′,6-diamidino-2-phenylindole (*DAPI*; nuclear) costaining images of 4T1 tumor slices from mice after different treatments indicated. Whereas tumors from untreated mice (*1st row*), Taxol-treated mice (*2nd row*), and plain SWNT-treated mice (*3rd row*) showed few apoptotic cells, many cells in the tumor from SWNT-PTX–treated mice (*4th row*) were undergoing apoptosis. *B,* Ki67 (proliferation assay) and DAPI costaining images of tumor slices from mice after various treatments. *4th row,* few proliferation active cells were observed in the tumor of mice that received SWNT-PTX treatment. Tumors used in this study were taken from 4T1 tumor-bearing mice 12 d after initiation of treatment. *Scale bar,* 100 μm.

(Fig. 2). The Ki67 antibody staining method has been widely used as a cell proliferation marker to stain proliferation active cells in the G_1, G_2, and S phases of the cell cycle (27). We found that cell proliferation in Taxol-treated tumor was as active as in untreated tumor (Fig. 3*B, 2nd row*; see Supplementary Fig. S5*B* for quantitative comparison). In the SWNT-PTX–treated tumor case, however, only ~20% of proliferation active cells were noted compared with the number in the untreated tumor ($P < 0.0001$ versus untreated and Taxol-treated tumors; Fig. 3*B, 3rd row*; Supplementary Fig. S5*B*). As the control, plain SWNT without PTX showed no effect to the tumors (Fig. 3, *3rd row*), proving that the treatment efficacy of SWNT-PTX is due to PTX carried into tumors by nanotubes. Thus, both TUNEL staining and Ki67 staining results clearly confirmed the treatment efficacy of SWNT-PTX by inhibiting proliferation and inducing apoptosis of tumor cells.

To investigate the pharmacokinetics of various drug complexes, we first measured blood circulation behaviors of PEGylated SWNTs with and without PTX conjugation by Raman spectroscopic detection of SWNTs in blood sample drawn from mice after injection of SWNT and SWNT-PTX (see Materials and Methods). We observed a significantly shortened circulation half-life of our branch-PEGylated SWNT from ~3.3 h to ~1.1 h (circulation half-life was obtained by one-compartment first-order exponential decay fitting; see Materials and Methods) after PTX conjugation (Fig. 4*A*). This result was important and attributed to the high hydrophobicity of conjugated PTX, reducing the biological inertness of the PEGylated nanotubes *in vivo* and shortening the blood circulation time. Blood circulation behaviors of the three forms of PTX were measured using ^{3}H-labeled PTX. Liquid scintillation counting of ^{3}H-PTX radioactivity of blood samples collected from mice after injection showed circulation half-lives of 18.8 ± 1.5, 22.8 ± 1.0, and 81.4 ± 7.4 min for ^{3}H-PTX injected in Taxol, PEG-PTX, and SWNT-PTX, respectively (Fig. 4*B*; see Supplementary Table S1 for complete pharmacokinetic data). This clearly revealed that conjugation of PTX to PEGylated SWNTs significantly increased the blood circulation time of PTX. Interestingly, simple PEGylation of PTX, through imparted water solubility of PTX, still exhibited much shorted blood circulation than PTX on PEGylated SWNTs. Note that for SWNT-PTX, circulation curves of radiolabeled PTX measured by radioactivity (Fig. 4*A* and *B, green curves*) and the drug carrier SWNT measured by Raman have consistent slopes (Fig. 4*A, red curve*), suggesting that PTX and SWNT remained in a conjugated form in the blood circulation stage, which is consistent to the relatively slow PTX releasing behavior of SWNT-PTX in mouse serum (Supplementary Fig. S2). The minor difference in the absolute values could be due to systematic errors between two different methodologies.

To understand the tumor treatment efficacy of various PTX formulations (i.e., SWNT-PTX, Taxol, and PEG-PTX), we investigated biodistribution of ^{3}H-PTX in the tumor and various main organs. We observed significant differences in the biodistribution of PTX administrated in the three formulations of PTX (Fig. 4*C* and *D*). Consistent with the blood circulation data (Fig. 4*B*), SWNT-PTX showed noticeable PTX activity in blood at 2 h after injection, whereas PTX levels in the blood were much lower in the Taxol ($P < 0.001$) and PEG-PTX ($P < 0.01$) cases (Fig. 4*C, inset*). Differences in biodistributions of PTX in the three cases were the most obvious at 2 h after injection, with much higher PTX signals in the RES organs (liver/spleen) and intestine of mice in the SWNT-PTX case than the two other cases (Fig. 4*C*).

Importantly, SWNT-PTX afforded much higher PTX uptake in the tumor than Taxol and PEG-PTX. The tumor PTX levels in the SWNT-PTX case were higher than those of Taxol and PEG-PTX by 10- and 6-fold, respectively, at 2 h after injection (Fig. 4*C*) and by 6- and 4-fold higher, respectively, at 24 h after injection ($P < 0.001$ in all cases; Fig. 4*D*). The ability of higher drug delivery efficiency to tumor by our PEGylated SWNTs was striking and directly responsible for the higher tumor suppression efficacy of SWNT-PTX than the other formulations. This suggests that to reach similar tumor uptake of drug, much lower injected dose can be used by SWNT delivery than Taxol, which is highly favorable for lowering toxic side effect to normal organs and tissues. An important gauge to drug delivery efficiency is the tumor-to-normal

organ/tissue PTX uptake ratios. We obtained significantly higher tumor-to-normal organ/tissue PTX uptake ratios (for tumor over liver, spleen, muscle, and other organs examined) in the case of SWNT-PTX than Taxol and PEG-PTX (except at 2 h after injection for spleen) at 2 and 24 h (Supplementary Table S2). This again makes SWNT-PTX highly favorable for high tumor suppression efficacy and low side effects.

We investigated the biodistribution of SWNTs injected as SWNT-PTX conjugates into mice by using their intrinsic Raman scattering properties without relying on radiolabel or fluorescent label (18, 28). We observed high uptake of SWNTs in the RESs (18–20), including liver and spleen (Fig. 5*A*–*C*). Tumor uptake of SWNT-PTX increased significantly from ~1% ID/g at 30 min to ~5% ID/g at 2 h, indicating accumulation of SWNT-PTX during this period through blood circulation (see Fig. 4*B* for circulation curve). Tumor uptake of SWNTs at 4.7% ID/g (SD = 2.1%, n = 3) was observed at 2 h after injection (Fig. 5*B*), reasonably consistent with the ~6.4% ID/g (SD = 1.1%, n = 3) PTX tumor uptake (Fig. 5*B*), suggesting that SWNT-PTX was taken up by tumor in a conjugated form. The SWNT biodistribution exhibited little change from 2 h (Fig. 5*B*) to 24 h after injection (Fig. 5*C*), in contrast to the biodistribution of radiolabeled PTX (Fig. 4*C* versus *D, green columns*). This suggests that the dissociation of PTX from SWNT carriers *in vivo* that resulted from *in vivo* cleavage of the ester bond between SWNT and PTX is likely by carboxylesterases (29–31).

We carried out micro-Raman imaging of SWNTs in tumor slices on sacrificing mice treated by SWNT-PTX at 24 h after injection. The tumor uptake of SWNTs was indeed confirmed by Raman mapping of the SWNT characteristic G-band Raman peak at

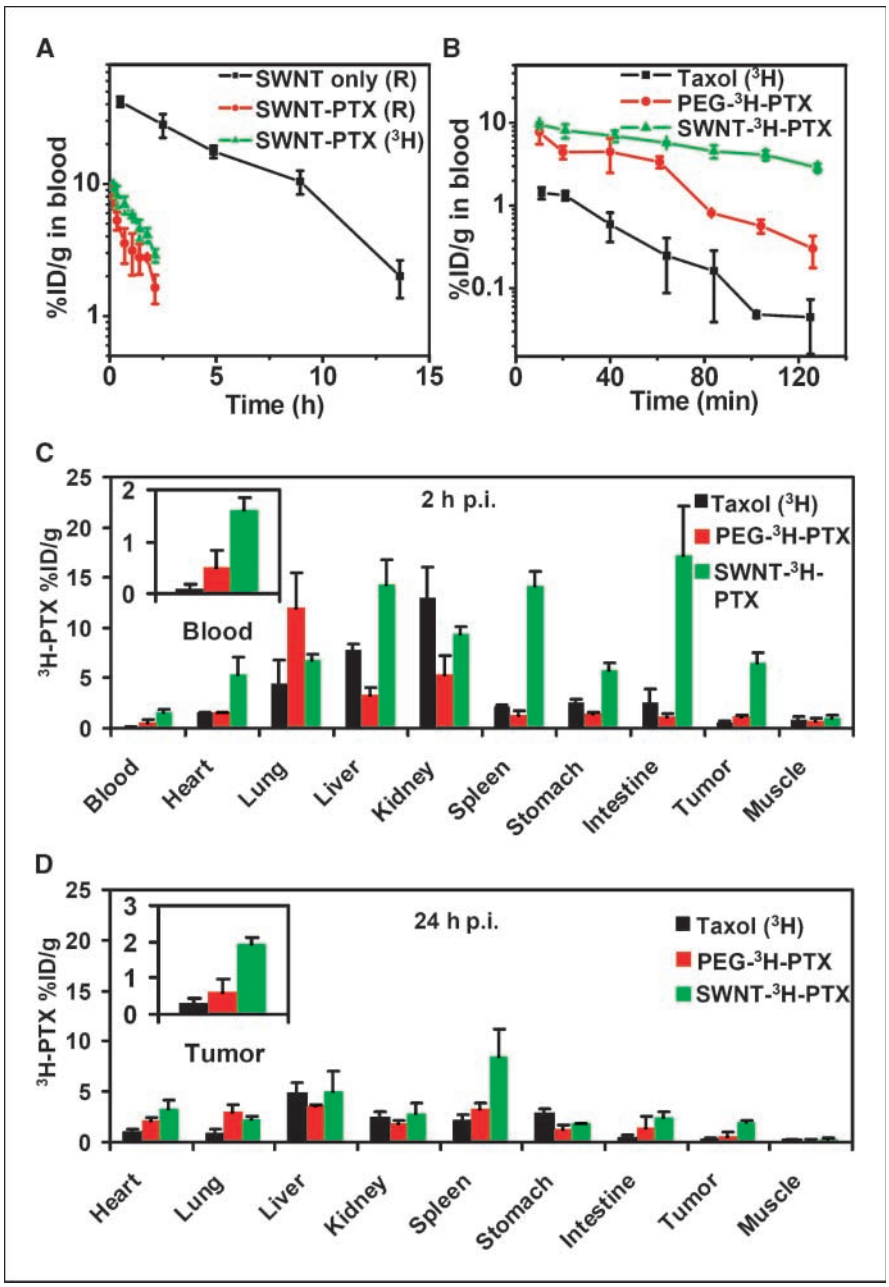

Figure 4. Pharmacokinetics and biodistribution. *A,* blood circulation data of SWNT with and without PTX conjugation [marked as *SWNT-PTX (R)* and *SWNT only (R)*, respectively] measured by Raman detection of SWNTs in blood samples (see Materials and Methods). Blood circulation data for SWNT-^{3}HPTX (*green curve*) were also obtained by scintillation counting of ^{3}H radioactivity in blood. Conjugation of PTX onto SWNTs greatly shortened circulation half-life of SWNTs from 3.3 to 1.1 h. *B,* blood circulation data of ^{3}H-labeled Taxol, PEG-PTX, and SWNT-PTX measured by scintillation counting. SWNT-PTX exhibited significantly prolonged circulation half-life (81.4 ± 7.4 min) than that of Taxol (18.8 ± 1.5 min) and PEG-PTX (22.8 ± 1.0 min). *C* and *D,* ^{3}H-PTX biodistribution in 4T1 tumor-bearing mice injected with ^{3}H-labeled Taxol, PEG-PTX, and SWNT-PTX at (*C*) 2 h after injection (*p.i.*) and (*D*) 24 h after injection. *Insets,* ^{3}H-PTX levels in the blood at 2 h after injection (*C*) and ^{3}H-PTX levels in the tumor at 24 h after injection (*D*). The error bars were based on three mice per group in all graphs. PTX dose (5 mg/kg) was used in all cases.

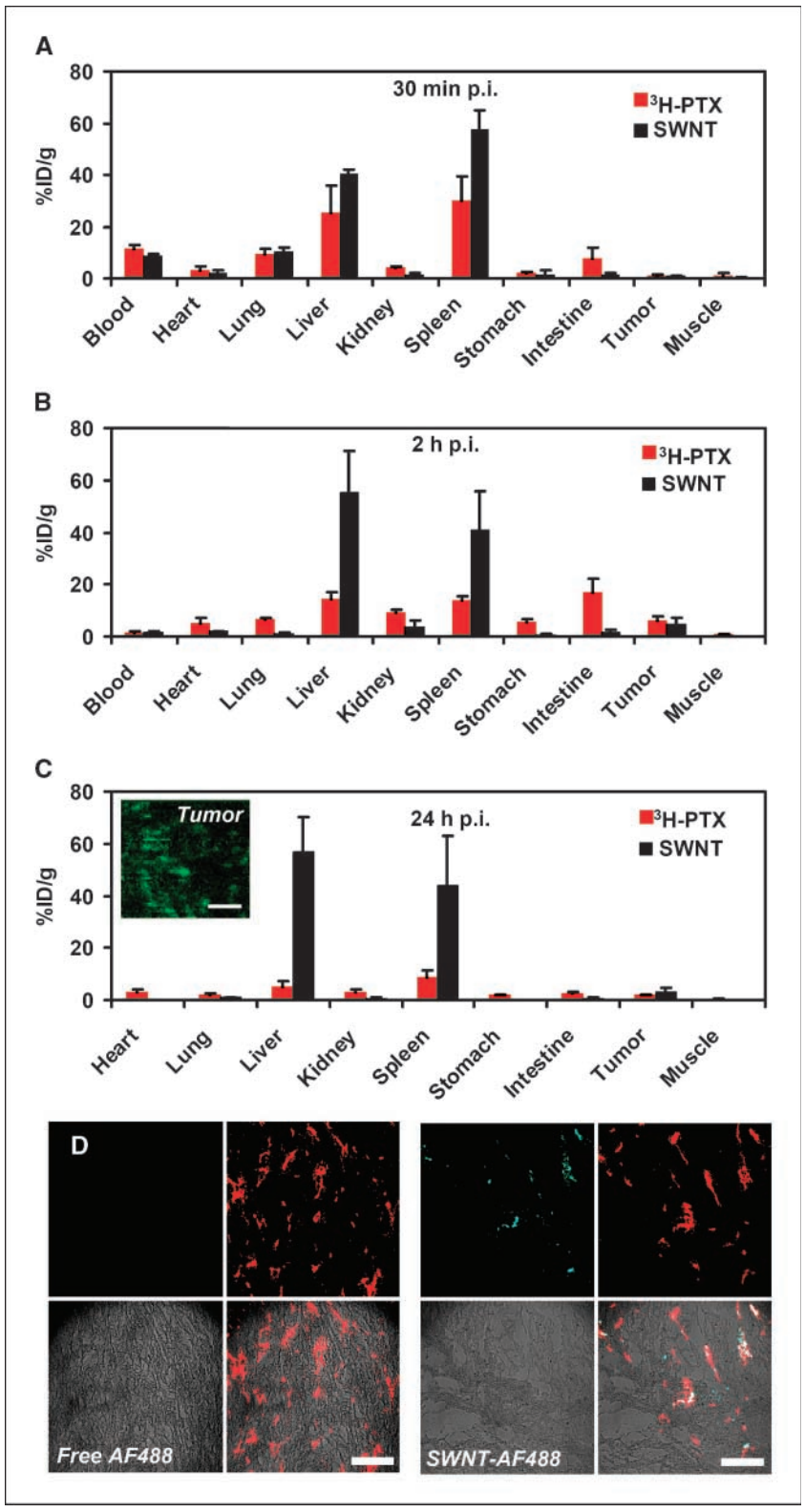

Figure 5. SWNT biodistribution measured by Raman spectroscopy. *A* to *C,* comparison of ^{3}H-PTX biodistribution and SWNT biodistribution in mice injected with SWNT-PTX(^{3}H) at 30 min (*A*), 2 h (*B*), and 24 h (*C*) after injection. SWNT biodistribution was measured by a Raman method (see Materials and Methods). The different biodistributions of PTX and SWNT carrier suggest rapid cleavage of ester bond for releasing of PTX from SWNTs *in vivo*. Error bars in all graphs were based on three mice per group. *C, inset,* a Raman image of the tumor slice. Strong SWNT G-band Raman signals at $\sim$1,580 cm^{-1} shift (*green* corresponds to high G-band intensity) were observed in the tumor. *Scale bar,* 50 μm. *D,* confocal fluorescence images of tumor slices from mice injected with free Alexa Fluor 488 (*AF488*) dye (*left*) and Alexa Fluor 488–labeled SWNT (*SWNT-AF488*; *right*). Tumor vasculature was stained by Cy3-anti-CD31. Alexa Fluor 488 fluorescence (*green*) and vasculature fluorescence (*red*) were overlaid with optical images. *Scale bar,* 100 μm.

$\sim$1,580 cm^{-1} in the tumor with a spatial resolution of $\sim$1 μm (Fig. 5*C, inset*). To investigate the location of nanotubes in the tumor relative to the vasculature, we injected Alexa Fluor 488 fluorescently labeled SWNTs into 4T1 tumor-bearing mice, sacrificed the mice, and collected the tumors for vasculature staining and fluorescence imaging (Fig. 5*D, right*). We observed fluorescently labeled SWNTs both with and without overlaying with tumor vasculatures. This suggested that although most SWNTs seemed to be located in or near the tumor vasculature, a fraction of nanotubes could leak through the tumor vessel into the tumor

interstitial space. As the control, no tumor retention of fluorescent dye was observed in mice injected with free Alexa Fluor 488 at the same dose (Fig. 5*D, left*).

Toxic side effects to normal organs and overall well being have been the main problems of cancer chemotherapeutics. By themselves, our well PEGylated SWNTs have been found to be nontoxic to mice *in vivo* monitored over many months (21, 22). We carried out a pilot toxicity study by treating healthy, tumor-free BALB/c mice with Taxol and SWNT-PTX at the same 5 mg/kg PTX dose once every 6 days. We observed neither mortality nor noticeable body weight loss of the mice treated with SWNT-PTX and Taxol compared with untreated control group at this relatively low PTX dose and injection frequency (Fig. 6*A*). Blood chemistry test was performed 24 days after initiation of the treatment, showing no physiologically significant difference among the three groups (Fig. 6*B*; Supplementary Table S3). Furthermore, H&E-stained sections of the 25 organs and organ systems were examined (Fig. 6*C*), without noticing obvious abnormal damage in the main organs including the liver and spleen that had high SWNT uptake, which was consistent to the normal hepatic enzyme levels measured in the blood chemistry test (Fig. 6*B*). The observed lack of obvious toxic side effect was partly due to the low dose of PTX used as the maximum tolerable dose of PTX in the Taxol case ~20 to 50 mg/kg (32–34). Achieving tumor treatment efficacy by SWNT-PTX at a PTX dose well below the toxic limit is owed to the ability of drug delivery to tumors by SWNTs. However, further careful studies, such as the hepatic macrophage function tests, are required to examine any potential near-term or long-term side effect of SWNT-PTX.

Discussion

We have shown that SWNT delivery of PTX affords markedly improved treatment efficacy over clinical Taxol, evidenced by its ability of slowing down tumor growth at a low PTX dose. The treatment effect is confirmed by tumor staining that reveals significant apoptotic cells and few proliferation active cells in the SWNT-PTX–treated tumor. The key reason for higher tumor suppression efficacy of SWNT-PTX than Taxol and PEG-PTX is the up to 10-fold higher tumor uptake of PTX afforded by SWNT carriers, which is a remarkable result. This is directly responsible for tumor suppression at a low dose of SWNT-PTX for the 4T1 tumor model normally resistant to PTX treatment (24).

Prolonged blood circulation and EPR effects are responsible for significantly higher tumor uptake of PTX in the SWNT-PTX case (6.4% ID/g at 2 h after injection) than Taxol (0.6% ID/g) and PEG-PTX (1.1% ID/g). The poor water solubility of various cancer therapeutic drugs limits their clinical applications. Cremophor EL is a commonly used reagent to disperse PTX and other drugs in saline for administration. However, its toxic effects have been noted in both animal models and patients (35–38). Similar to previous reports (39–44), we observe (Fig. 4*B*) short blood circulation time for PTX in Taxol. Little PTX (<2% ID/g) in the

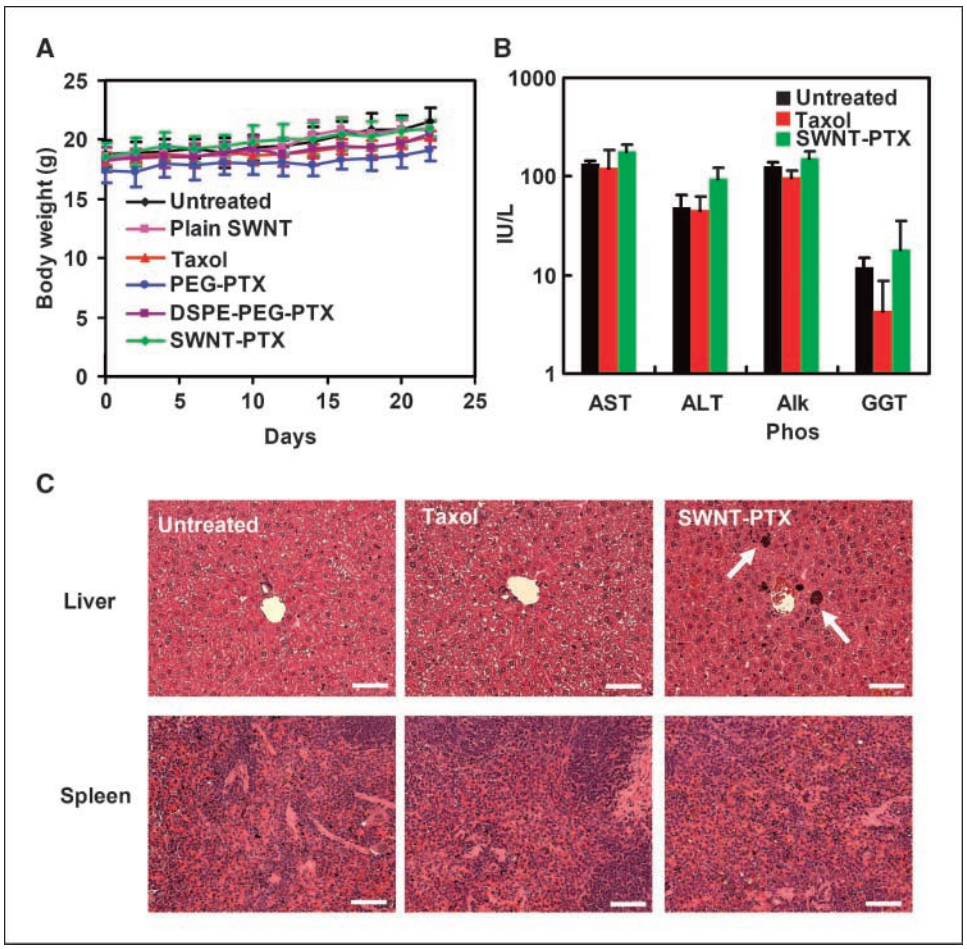

Figure 6. Pilot toxicity study. *A,* body weight curves of mice that received different treatments in the study (PTX dose, ~5 mg/kg). No obvious loss of body weight was observed in all the groups. Five to 14 mice were used in each group (see details in Fig. 2 caption). *B,* blood chemistry data of untreated, Taxol-treated, and SWNT-PTX–treated mice. Specific attention was paid to those hepatic-related serum chemistries (which would reflect liver damage or alternation of function), including aspartate aminotransferase (*AST*), alanine transaminase (*ALT*), alkaline phosphatase (*Alk Phos*), and γ-glutamyl transpeptidase (*GGT*), without finding obvious abnormality for SWNT-PTX–treated mice. The error bars are based on three mice in each group. *C,* H&E-stained liver and spleen slices of mice. Although residues of carbon nanotubes were observed as black dots in the liver as pointed by the white arrow, no obvious damage was noticed in the liver and spleen of SWNT-PTX–treated mice. *Scale bar,* 50 μm.

Taxol form remains circulating in the blood after only 11 min after injection at the current 5 mg/kg injected dose (Fig. 4*B*). PTX in Taxol is cleared from the blood and taken up by various organs especially kidney and liver for rapid renal and fecal excretion with very low tumor uptake (39–41, 43).

Branched PEGylation of PTX via similar ester linkage as in SWNT-PTX conjugates affords water solubility of PTX. However, the blood circulation time is still short (PEG-PTX concentration diminished to <2% ID/g in ~70 min after injection), albeit longer than Taxol. PEG-PTX remains a relatively small molecule that tends to be rapidly excreted via the kidney and renal route, evidenced by the high kidney and urine signals of radiolabeled PEG-PTX (data not shown). This leads to little advantage of PEGylation of PTX over Taxol in tumor uptake and treatment efficacy, as found here and by previous PTX PEGylation work (45).

The water solubility of our SWNT-PTX formulation favors prolonged blood circulation. Nevertheless, the high hydrophobicity of PTX reduces the hydrophilicity and biological inertness of our branch PEG functionalized SWNTs, causing significantly shortened blood circulation half-lives of the SWNT-PTX formulation (~1.1 h) compared with PEGylated SWNTs without PTX attachment (~3.3 h; Fig. 4*A*). The higher hydrophobicity led to increased nonspecific protein absorption on the nanotube conjugates, which accelerated the uptake by macrophages in RES organs. Compared with PEG-PTX, SWNT-PTX exhibits finite lengths (20–300 nm; mean, ~100 nm; Supplementary Fig. S1), a factor that favors long blood circulation because the average length of the nanotubes exceeds the threshold for renal clearance (46). Pharmacokinetics of materials with long blood circulation times are typically desired for a drug delivery vehicle for tumor treatment (2, 47, 48) to favor high tumor accumulation from the circulating blood through EPR effects. Note that our method of drug delivery by PEGylated SWNTs should be readily applicable to a wide range of hydrophobic or water-insoluble drugs. This could lead to a general drug delivery strategy for potent but water-insoluble molecules.

Tumor staining data clearly revealed apoptotic cells (Fig. 3*A*) inside the tumor treated by SWNT-PTX. Nanotubes were observed in the tumor vasculature as well as leaked out of the vessels (Fig. 5*D, left*). Drug delivery to cancer cells through the tumor vessel walls and interstitial space is desired for high tumor treatment efficacy. SWNTs seemed to exhibit certain ability in overcoming these barriers, which could be related to the quasi one-dimensional shape of these materials. An interesting feature of SWNTs is that the length of nanotubes (20–300 nm currently) could be controlled more precisely to span various size regimens. This could allow for investigation of length effect of one-dimensional materials to the tumor penetration and suppression efficacy of drug complexes. This intriguing length effect will require systematic exploration in the future.

PTX conjugation to PEGylated SWNTs clearly alters the pharmacokinetics and biodistribution of PTX from Taxol and PEG-PTX. The up to 10 times high tumor uptake of the drug through SWNT-PTX and high tumor-to-normal organ/tissue PTX uptake ratios strongly favor high tumor killing efficacy and low toxicity to normal organs. High RES uptake is known for nanomaterials in general. The high uptake of SWNT-PTX in RES organs such as liver and spleen (18, 22) could be a cause of concern in terms of toxicity to these organs. Importantly, our biodistribution studies revealed relatively low PTX levels in the RES organs at later time points (2 and 24 h), differing from the SWNT biodistribution (Fig. 5*A–C*). The difference between the biodistribution of SWNT and ^{3}H-PTX (measured by radioactivity) suggests rapid release of PTX from SWNT in the various organs and tissues *in vivo*, resulted from *in vivo* cleavage of the ester linkage between PTX and PEGylated SWNT most likely by carboxylesterases especially those in the liver (29–31). We observed a significant PTX accumulation but proportionally lower SWNT signal in the intestine in the PTX-SWNT case at 30 min and 2 h after injection (Fig. 5*A* and *B*). We also detected strong PTX signal in the feces even at only 30 min after injection (data not shown). These data suggested that SWNT-PTX taken up by the RES organs was dissociated via ester cleavage for release for excretion. Unlike the SWNT carriers, which are excreted gradually in weeks or even months (22), the dissociated PTX drug molecules can be rapidly excreted via both feces and urine without causing noticeable toxicity. Taken together, the uptake of drug-nanomaterial complexes by RES could serve as a scavenger system to eliminate toxic drugs as well as carriers.

The maximum tolerable dose of Taxol for BALB/c mice is reported to be in the range of 20 to 50 mg/kg (32–34). Achieving tumor growth suppression by SWNT-PTX at 5 mg/kg dose once every 6 days suggests the promise of SWNT drug delivery for effective cancer treatment with low side effects. More importantly, our water-soluble SWNT-PTX formulation is Cremophor-free. SWNTs have shown to be safe at least in mouse models (21, 22). The amount of SWNTs required to give 5 mg/kg PTX is only ~4 mg/kg compared with ~420 mg/kg Cremophor in the Taxol case for the same PTX dose. Further, the same SWNT conjugation strategy applies to many other water-insoluble drugs.

SWNTs are highly promising for drug delivery due to several factors. These materials can now be functionalized to a sufficient degree to facilitate nearly complete excretion of SWNTs from mice over time (22). The chemical composition (purely carbon) of carbon nanotubes is among the safest in the inorganic nanomaterials, many of which such as quantum dots have heavy metal compositions. The unique one-dimensional structure and tunable length provide an ideal platform to investigate size and shape effects *in vivo*. Lastly, unlike the conventional organic drug carriers, the intrinsic spectroscopic properties of nanotubes, including Raman and photoluminescence, can provide valuable means of tracking, detecting, and imaging to understand the *in vivo* behavior and drug delivery efficacy *in vivo*. Taken together, carbon nanotubes are promising materials for potential multimodality cancer therapy and imaging.

To our knowledge, this is the first successful report that carbon nanotubes are used as drug delivery vehicles to achieve *in vivo* tumor treatment efficacy with mice. This opens up further exploration of biomedical applications of novel carbon nanomaterials with animals for potential translation into the clinic in the future. It is important to note that nanotube functionalization chemistry largely determines the efficacy of SWNT drug delivery, as our various other functionalization attempts have failed to give satisfactory treatment efficacy in other experiments. The treatment efficacy of SWNT-based drug delivery vehicles can be further improved because the current functionalization scheme is not yet fully optimized. Targeting ligands on nanotubes for tumor-targeted drug delivery is also expected to further enhance treatment efficacy. The one-dimensional shape and length of nanotubes easily allow for targeting ligands, drugs, and multiple molecules for synergistic effects.

Disclosure of Potential Conflicts of Interest

No potential conflicts of interest were disclosed.

Acknowledgments

Received 4/19/2008; revised 5/27/2008; accepted 5/28/2008.

Grant support: NIH-National Cancer Institute Center for Cancer Nanotechnology Excellence Focused on Therapeutic Response at Stanford (H. Dai), Stanford Bio-X Initiative Grant, NIH-National Cancer Institute R01 grant CA135109-01, and Stanford Graduate Fellowship.

The costs of publication of this article were defrayed in part by the payment of page charges. This article must therefore be hereby marked *advertisement* in accordance with 18 U.S.C. Section 1734 solely to indicate this fact.

We thank Josher Robinson for the help in dynamic light scattering experiments.

References

1. Langer R. Drug delivery and targeting. Nature 1998; 392:5–10.
2. Moghimi SM, Hunter AC, Murray JC. Long-circulating and target-specific nanoparticles: theory to practice. Pharmacol Rev 2001;53:283–318.
3. Maeda H, Wu J, Sawa T, Matsumura Y, Hori K. Tumor vascular permeability and the EPR effect in macromolecular therapeutics: a review. J Cont Rel 2000; 65:271–84.
4. Gao XH, Cui YY, Levenson RM, Chung LWK, Nie SM. *In vivo* cancer targeting and imaging with semiconductor quantum dots. Nat Biotechnol 2004;22:969–76.
5. Bartlett DW, Su H, Hildebrandt IJ, Weber WA, Davis ME. Impact of tumor-specific targeting on the biodistribution and efficacy of siRNA nanoparticles measured by multimodality *in vivo* imaging. Proc Natl Acad Sci U S A 2007;104:15549–54.
6. Iyer AK, Khaled G, Fang J, Maeda H. Exploiting the enhanced permeability and retention effect for tumor targeting. Drug Discov Today 2006;11:812–8.
7. Feazell RP, Nakayama-Ratchford N, Dai H, Lippard SJ. Soluble single-walled carbon nanotubes as longboat delivery systems for platinum(IV) anticancer drug design. J Am Chem Soc 2007;129:8438–9.
8. Liu Z, Sun X, Nakayama N, Dai H. Supramolecular chemistry on water-soluble carbon nanotubes for drug loading and delivery. ACS Nano 2007;1:50–6.
9. Bianco A, Kostarelos K, Prato M. Applications of carbon nanotubes in drug delivery. Curr Opin Chem Bio 2005;9:674–9.
10. Pantarotto D, Briand JP, Prato M, Bianco A. Translocation of bioactive peptides across cell membranes by carbon nanotubes. Chem Comm 2004;16–7.
11. Kam NWS, Dai H. Carbon nanotubes as intracellular protein transporters: generality and biological functionality. J Am Chem Soc 2005;127:6021–6.
12. Liu Y, Wu DC, Zhang WD, et al. Polyethyleniminegrafted multiwalled carbon nanotubes for secure noncovalent immobilization and efficient delivery of DNA. Angew Chem Int Ed 2005;44:4782.
13. Kam NWS, Liu Z, Dai H. Functionalization of carbon nanotubes via cleavable disulfide bonds for efficient intracellular delivery of siRNA and potent gene silencing. J Am Chem Soc 2005;36:12492–3.
14. Liu Z, Winters M, Holodniy M, Dai H. siRNA delivery into human T cells and primary cells with carbon-nanotube transporters. Angew Chem Int Ed 2007;46: 2023–7.
15. Kam NWS, Liu Z, Dai H. Carbon nanotubes as intracellular transporters for proteins and DNA: an investigation of the uptake mechanism and pathway. Angew Chem Int Ed 2006;45:577–81.
16. Kam NWS, O'Connell M, Wisdom JA, Dai H. Carbon nanotubes as multifunctional biological transporters and near-infrared agents for selective cancer cell destruction. Proc Natl Acad Sci U S A 2005;102:11600–5.
17. Welsher K, Liu Z, Daranciang D, Dai H. Selective probing and imaging of cells with single walled carbon nanotubes as near-infrared fluorescent molecules. Nano Lett 2008;8:586–90.
18. Liu Z, Cai W, He L, et al. *In vivo* biodistribution and highly efficient tumour targeting of carbon nanotubes in mice. Nat Nanotechnol 2007;2:47–52.
19. Cherukuri P, Gannon CJ, Leeuw TK, et al. Mammalian pharmacokinetics of carbon nanotubes using intrinsic near-infrared fluorescence. Proc Natl Acad Sci U S A 2006;103:18882–6.
20. McDevitt MR, Chattopadhyay D, Kappel BJ, et al. Tumor targeting with antibody-functionalized, radiolabeled carbon nanotubes. J Nucl Med 2007;48:1180–9.
21. Schipper ML, Nakayama-Ratchford N, Davis CR, et al. Pilot toxicology study of single-walled carbon nanotubes in a small sample of mice. Nat Nanotechnol 2008; 3:216–21.
22. Liu Z, Davis C, Cai W, He L, Chen X, Dai H. Circulation and long-term fate of functionalized, biocompatible single-walled carbon nanotubes in mice probed by Raman spectroscopy. Proc Natl Acad Sci U S A 2008;105:1410–5.
23. Deutsch HM, Glinski JA, Hernandez M, et al. Synthesis of congeners and prodrugs. 3. Water-soluble prodrugs of taxol with potent antitumor activity. J Med Chem 1989;32:788–92.
24. Janat-Amsbury MM, Yockman JW, Lee M, et al. Combination of local, nonviral IL12 gene therapy and systemic paclitaxel treatment in a metastatic breast cancer model. Mol Ther 2004;9:829–36.
25. Janat-Amsbury MM, Yockman JW, Lee M, et al. Local, non-viral IL-12 gene therapy using lipopolymer as carrier system combined with a water soluble systemic paclitaxel for cancer treatment. J Cont Rel 2005; 101:273–85.
26. Inbal B, Cohen O, PolakCharcon S, et al. DAP kinase links the control of apoptosis to metastasis. Nature 1997; 390:180–4.
27. Langford LA, Cooksley CS, DeMonte F. Comparison of MIB-1 (Ki-67) antigen and bromodeoxyuridine proliferation indices in meningiomas. Hum Pathol 1996;27:350–4.
28. Rao AM, Richter E, Bandow S, et al. Diameter-selective Raman scattering from vibrational modes in carbon nanotubes. Science 1997;275:187–91.
29. Satoh T, Hosokawa M. The mammalian carboxylesterases: from molecules to functions. Annu Rev Pharmacol Toxicol 1998;38:257–88.
30. Guengerich FP, Peterson LA, Bocker RH. Cytochrome-P-450-catalyzed hydroxylation and carboxylic-acid ester cleavage of Hantzsch pyridine esters. J Biol Chem 1988;263:8176–83.
31. Morgan EW, Yan B, Greenway D, Petersen DR, Parkinson A. Purification and characterization of two rat liver microsomal carboxylesterases (hydrolase A and B). Arch Biochem Biophys 1994;315:495–512.
32. Le Garrec D, Gori S, Luo L, et al. Poly(*N*-vinylpyrrolidone)-block-poly(D,L-lactide) as a new polymeric solubilizer for hydrophobic anticancer drugs: *in vitro* and *in vivo* evaluation. J Control Release 2004;99:83–101.
33. Sugahara S, Kajiki M, Kuriyama H, Kobayashi TR. Paclitaxel delivery systems: the use of amino acid linkers in the conjugation of paclitaxel with carboxymethyldextran to create prodrugs. Biol Pharm Bull 2002;25:632–41.
34. Sharma A, Straubinger RM. Novel taxol formulations: preparation and characterization of taxol-containing liposomes. Pharm Res 1994;11:889–96.
35. Liebmann J, Cook JA, Mitchell JB. Cremophor EL, solvent for paclitaxel, and toxicity. Lancet 1993;342:1428.
36. Ellis AG, Crinis NA, Webster LK. Inhibition of etoposide elimination in the isolated perfused rat liver by Cremophor EL and Tween 80. Cancer Chemother Pharmacol 1996;38:81–7.
37. Gelderblom H, Verweij J, Nooter K, Sparreboom A. Cremophor EL: the drawbacks and advantages of vehicle selection for drug formulation. Eur J Cancer 2001;37:1590–8.
38. Arbuck SG, Strauss H, Rowinsky E, et al. A reassessment of cardiac toxicity associated with Taxol. J Natl Cancer Inst Monogr 1993;15:117–30.
39. Eiseman JL, Eddington ND, Leslie J, et al. Plasma pharmacokinetics and tissue distribution of paclitaxel in CD2F1 mice. Cancer Chemother Pharmacol 1994;34: 465–71.
40. Sparreboom A, van Tellingen O, Nooijen WJ, Beijnen JH. Tissue distribution, metabolism and excretion of paclitaxel in mice. Anticancer Drugs 1996;7:78–86.
41. Gangloff A, Hsueh WA, Kesner AL, et al. Estimation of paclitaxel biodistribution and uptake in human-derived xenografts *in vivo* with (18)F-fluoropaclitaxel. J Nucl Med 2005;46:1866–71.
42. Sparreboom A, van Tellingen O, Nooijen WJ, Beijnen JH. Nonlinear pharmacokinetics of paclitaxel in mice results from the pharmaceutical vehicle Cremophor EL. Cancer Res 1996;56:2112–5.
43. Yeh TK, Lu Z, Wientjes MG, Au JL. Formulating paclitaxel in nanoparticles alters its disposition. Pharm Res 2005;22:867–74.
44. Chen XY, Plasencia C, Hou YP, Neamati N. Synthesis and biological evaluation of dimeric RGD peptide-paclitaxel conjugate as a model for integrin-targeted drug delivery. J Med Chem 2005;48:1098–106.
45. Li C, Yu D, Inoue T, et al. Synthesis and evaluation of water-soluble polyethylene glycol-paclitaxel conjugate as a paclitaxel prodrug. Anticancer Drugs 1996;7:642–8.
46. Soo Choi H, Liu W, Misra P, et al. Renal clearance of quantum dots. Nat Biotechnol 2007;25:1165–70.
47. Allen TM, Hansen C, Rutledge J. Liposomes with prolonged circulation times: factors affecting uptake by reticuloendothelial and other tissues. Biochim Biophys Acta 1989;981:27–35.
48. Gabizon A, Papahadjopoulos D. Liposome formulations with prolonged circulation time in blood and enhanced uptake by tumors. Proc Natl Acad Sci U S A 1988;85:6949–53.

Drug Delivery with Carbon Nanotubes for *In vivo* Cancer Treatment

Zhuang Liu, Kai Chen, Corrine Davis, et al.

Cancer Res 2008;68:6652-6660.